BULLETIN OF THE POLISH ACADEMY OF SCIENCES
TECHNICAL SCIENCES, Vol. 61, No. 1, 2013
DOI: 10.2478/bpasts-2013-0020

Theoretical modelling of MWIR thermoelectrically cooled nBn HgCdTe detector

P. MARTYNIUK* and A. ROGALSKI

Institute of Applied Physics, Military University of Technology, 2 Kaliskiego St., 00-908 Warsaw, Poland

Abstract. The paper reports on the medium wavelength infrared (MWIR) unipolar barrier infrared detector (UBIRD) nBn/B-n type (n-type barrier) HgCdTe detector's photoelectrical performance. The UBIRD nBn/B-n type HgCdTe detector was modelled using commercially available software APSYS. Detailed analysis of the detector's performance (such as dark current, photocurrent, responsivity, and detectivity) versus bias voltage, operating temperatures, and structural parameters (cap, barrier, and absorber's doping as well as cap and barrier compositions) were performed pointing out optimal working conditions. Both conduction and valence band alignments of the HgCdTe nBn/B-n type detector structure was simulated stressing their importance on detectors performance. It was shown that higher operation temperature (HOT) conditions achieved by commonly used thermoelectric (TE) coolers allow to obtain detectivities of D^* = (3–10)$\times 10^9$ cmHz$^{1/2}$/W at $T = 200$ K for detectors with cut-off wavelength of 5.2 μm The differential resistance area product of *RA* = 0.15–0.4 cm^2 at $T = 230$ K for bias voltage $V = 50$ mV was estimated.

Finally, the state of the art of UBIRD HgCdTe nBn/B-n type detector performance was compared to InAs/GaSb/B-$Al_{0.2}Ga_{0.8}Sb$ T2SLs nBn detector, InAs/GaSb T2SLs PIN and the HOT HgCdTe bulk photodiodes' operated at near-room temperature ($T = 230$ K). It was shown that the *RA* product of the MWIR UBIRD nBn/B-n type HgCdTe detector can reach a comparable level to the state of the art of the HgCdTe HOT bulk photodiodes and two types of type-II superlattice detectors: PIN photodiodes and nBn detectors.

Key words: barrier detectors, unipolar barrier, nBn, HgCdTe, photodetectors.

1. Introduction

As of now, the infrared (IR) photodetector technology is dominated by HgCdTe photodiodes [1–3]. The narrow band gap IR detectors requires cryogenic cooling to suppress the dark current, which is typically limited by Auger generation-recombination (GR) and Shockley-Read-Hall (SRH) processes. The necessity of the IR detectors' cryogenic cooling is a major obstacle preventing their widespread applications. The increasing of detector's operating temperature without sacrificing its performance remains to be a crucial objective of the research groups.

Among the mechanisms generating the dark current in detector's structure the following must be enumerated: diffusion and GR mechanisms, band-to-band (BTB) tunnelling, trap assisted tunnelling (TAT), and leakage currents. The incorporation of type-II InAs/GaSb superlattices (T2SLs) of 6.1 Å $A^{III}B^{V}$ semiconductor family into detector architecture allows reducing the adverse BTB/TAT currents and contribution of Auger mechanism to the total dark current. Therefore T2SLs could be considered as an alternative to the bulk HOT HgCdTe detectors [4]. Unfavourable GR and leakage dark current components can be limited by the properly selected barriers incorporated into detectors structure. The barrier's selection plays crucial role due to the lattice constant matching of the detectors constituent layers. The barrier's height in both conduction and valence bands connect directly to the band alignments. It must be stressed that band alignment playing important role in construction of the barrier IR structures is often fortuitous and extremely difficult to control from technological perspective [5].

The very first barrier structures were commonly known $A^{II}B^{VI}$ and $A^{III}B^{V}$ heterostructures invented to increase device's performance by suppression of the diffusion currents from the detector's active region. The next stage in IR detector's development was double layer heterojunction (DLHJ) allowing reducing both majority and minority carriers diffusion currents in comparison to the homojunction IR detectors [6]. Currently, among the barrier IR detectors (BIRD) the leading position is occupied by UBIRD constructed with $A^{III}B^{V}$ compounds (GaSb, $InAs_{1-z}Sb_z$ – cap layers, $InAs_{1-y}Sb_y$ – active region, $AlSb_{1-x}As_x$ – barrier), T2SL nBn InAs/GaSb detector with AlGaSb barrier and HgCdTe [7]. The idea of the UBIRD structure and its potential HOT capabilities were proposed by Maimon and Wicks [8]. They pointed out that introducing of unipolar barriers in detector structure drastically change the architecture of infrared detectors and their physical properties. Unipolar barriers are used to impede the flow of majority carrier dark current in photoconductors thus nBn structure operates as a minority carrier device.

As stated above, the potential interest in InAs/GaSb T2SLs results from unique inherited capabilities of this new artificial material with completely different physical properties in comparison to the constituent layers (InAs and GaSb). Electronic properties of T2SLs may be superior to those of the HgCdTe alloy. The effective masses are not directly dependent on the band gap energy, as it is in the case of bulk semiconductor.

*e-mail: pmartyniuk@wat.edu.pl

The electron effective mass of InAs/GaInSb SL ($m^*/m_o \approx$ 0.02–0.03) is larger compared to m^*/m_o = 0.009 in HgCdTe alloy with the same band gap $E_g \approx 0.1$ eV. Thus, diode tunnelling currents in the SL can be reduced compared to the HgCdTe alloy. Due to spatial separations of electrons and holes, the Auger recombination rates in T2SLs are suppressed by several orders, compared to those of bulk HgCdTe with similar band-gap. Finally, 6.1 Å $A^{III}B^{V}$ family allows nearly zero band offsets leading to the desirable UBIRD band alignments difficult to attain in HgCdTe [9].

Although abovementioned physical properties indicates potential T2SLs' superiority over bulk materials (including HgCdTe), similarly to quantum dot infrared detectors (QDIP $\eta < 10\%$), T2SLs' quantum efficiency leaves a lot of to be desired ($\eta = 20$–30%) which stems from technological problems connected with growth of uniform and thick enough SLs allowing proper electron and hole wavefunctions overlapping [10, 11]. It is commonly known that bulk HgCdTe offers quantum efficiency about 70% and lattice matching capabilities, therefore recently, one research group has attempted to apply UBIRD nBn architecture to HgCdTe alloy which should offer potential and theoretical advantages over p-n HgCdTe homojunction [12, 13]. Additionally, UBIRD (with B-n type barrier) architecture should circumvent problems with attaining a proper level of the p type doping and simplify the fabrication process (e.g. annealing).

In this paper we present the performance of the MWIR HgCdTe detector with cut-off wavelength of $\lambda_c = 5.2$ μm at $T = 200$ K. The temperature and bias voltage dependences of the dark current, *RA* product, responsivity and detectivity of the nBn UBIRD HgCdTe/B-n type detector are analysed. Finally, the state of the art of near-room temperature MWIR UBIRD nBn/B-n type HgCdTe detector performance is compared to InAs/GaSb/B-$Al_{0.2}Ga_{0.8}Sb$ T2SLs nBn, InAs/GaSb T2SL PIN and HOT HgCdTe bulk photodiodes' ones.

2. Simulation procedure

The detailed description of the growth procedure and device's characterization could be found in the paper by Velicu e*t al.* [13]. For modelling purposes three layers barrier was applied in order to mitigate the kinks emerging in energy band diagrams between detector's constituent layers. In addition, three layer barrier was utilized to simulate potential issues with compositional uniformity at the interfaces. The interdiffusion was modelled by applying gauss tail doping (dx = 0.05 μm).

The modelled structure shown in Fig. 1 consists of the n-type HgCdTe absorber with a thickness 2.79–10 μm doped with In ($n = 10^{14}$ cm^{-3}) and composition $x = 0.275$ for MWIR range. After the absorber layer, an $n$type HgCdTe barrier was grown with a thickness of 0.15 μm doped with In ($n = 2 \times 10^{15}$ cm^{-3}). As mentioned, in our model the barrier layer was divided on three sublayers with composition grading fitted to the cap layer and absorber respectively (e.g. $x = 0.33$–0.6–0.275). The barrier thickness was assumed to be thick enough to prevent electron tunnelling between the top contact layer and the absorbing layer – therefore, the majority current is blocked by the barrier material under an applied bias. Finally, the 0.16 μm thick n-type doped with In ($n = 7 \times 10^{14}$ cm^{-3}) HgCdTe cap layer was grown.

The numerical calculations were performed utilizing commercial software APSYS. Specific equations and relations used in device's modelling are listed in Table 1 and Appendix. The 50% cut-off wavelength was calculated to be $\lambda_c = 5.2$ μm at $T = 200$ K. The detector's area equals 120×120 μm^2.

The noise current was calculated using the expression including Johnson-Nyquist noise, optical and electrical shot noises:

$$i_n(V) = \sqrt{(4k_BT/RA) + 2qI_{DARK} + 2qI_{SCENE}}, \quad (1)$$

where A is a detector's area, *RA* – dynamic resistance area product, I_{DARK} and I_{SCENE} are the dark current density and background induced current, respectively, and k_B is the Boltzmann constant.

The background wavelength dependent current was calculated according to the expression:

$$I_{SCENE} = \frac{2\pi cq}{\lambda^4} \sin^2\left(\frac{\theta}{2}\right) \int_0^{\lambda_c} (\exp(hc/k_BT_s\lambda) - 1)^{-1} \eta(\lambda) d\lambda, \quad (2)$$

where T_s is a scene temperature, θ – detector's field of view ($\theta = 20°$), and $T_s = 300$ K was assumed.

The quantum efficiency was calculated as a function of the incident wavelength and current responsivity, R_i, according to the relation:

$$\eta(\lambda) = 1.24 \frac{R_i}{\lambda}. \quad (3)$$

The detector's detectivity was defined by expression:

$$D^* = \frac{R_i}{i_n(V)} \sqrt{A}. \quad (4)$$

The very first experimental results related to the MWIR UBIRD nBn/B-n type IR detectors were presented recently by Velicu *et al.* [11]. Figure 2 depicts the simulated dark current versus reverse bias for selected operating temperatures which could be obtained by TE cooling. The barrier's influence is clearly evident in calculated dark current-voltage characteristics, where "turn-on" voltage (indicates the voltage required to minimize valence band barrier) was assumed to be $V = 0.4$ V. The inset compares simulation results of the structure presented in Fig. 1 with the experimental data presented in Ref. 13. Within the operating temperature range, $T = 180$–240 K, the dark current increases from 0.4 to 7 A/cm^2 while corresponding detectivities change from 1×10^9 to 6.5×10^9 cmHz$^{1/2}$/W at $\lambda = 4.9$ μm, respectively (see Fig. 3). It was shown that for voltages $V < 300$ mV the dark current increases sharply (hole concentration increases harshly), while above $V > 0.3$ V typical photoconductive effect related to the increase of the current versus bias is observed. UBIRD nBn HgCdTe/B-n type structure operates in minority carrier manner thus dark current is mainly due to the hole transport from absorber's layer.

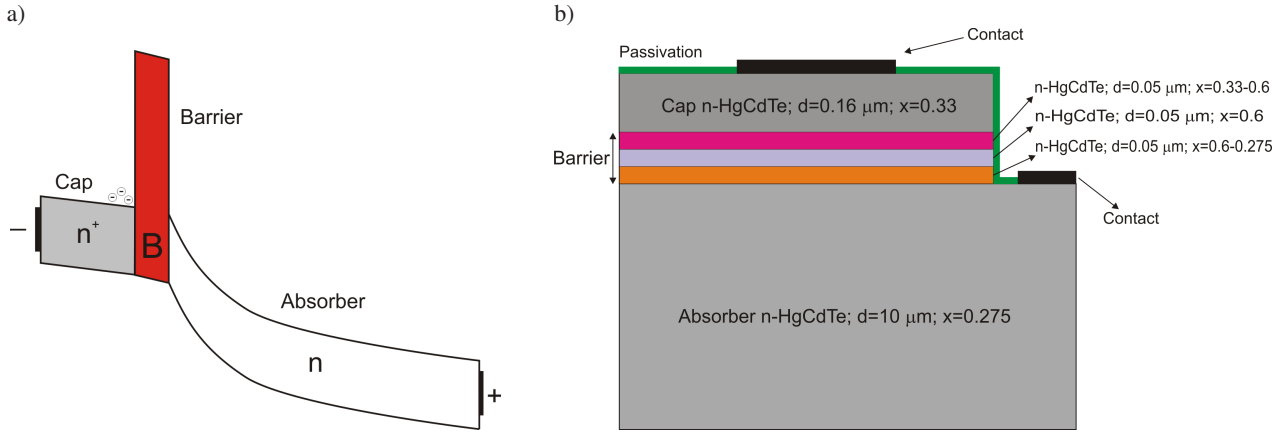

Fig. 1. UBIRD detector with the nBn design: a) heterostructure schematic of the device, b) device's structure

Table 1
Parameters taken in modelling of MWIR UBIRD nBn HgCdTe/B-n type detectors

	Cap	Barrier	Absorber
Donor concentration, N_D [cm^{-3}]	$10^{14} \rightarrow 5 \times 10^{16}$	1014?5 1016	1014?5 1016
Doping concentration's gauss tail, dx [μm]	0.05		
Composition, x [μm]	$0.15 \rightarrow 0.5$	$0.33 \rightarrow 0.7 \rightarrow 0.275$	0.275 ($\lambda_c = 5.2$ μm at $T = 200$ K)
Geometry, d [μm]	$0.16 \rightarrow 1$	$0.06 \rightarrow 0.15$	$5 \rightarrow 10$
Device electrical area, A [μm^2]	120×120		
Background temperature, T_s, field of view, θ	300 K, 20° ($f = 2.835$)		
Overlap matrix F_1F_2	0.2		
Trap energy level, E_{Trap}	$E_g/2$		
Trap concentration, N_{Trap} [cm^{-3}]	10^{16}		
Minority carrier lifetime SHR, τ_n, τ_p [μs]	0.4, 1		
Incident power density, Φ [W/m^2]	50×10^4		

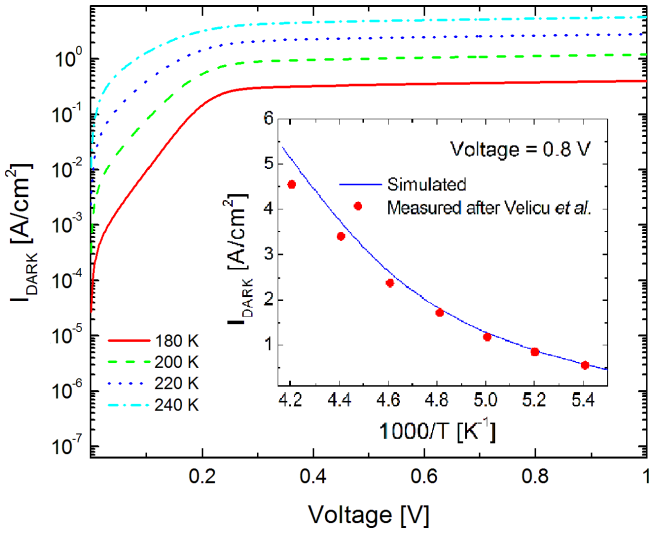

Fig. 2. I_{DARK} versus voltage for UBIRD nBn HgCdTe/B-n detector ($\lambda_c = 5.2$ μm at $T = 200$ K) for selected operating temperatures. Inset: comparison with experimental results presented by Ref. 13

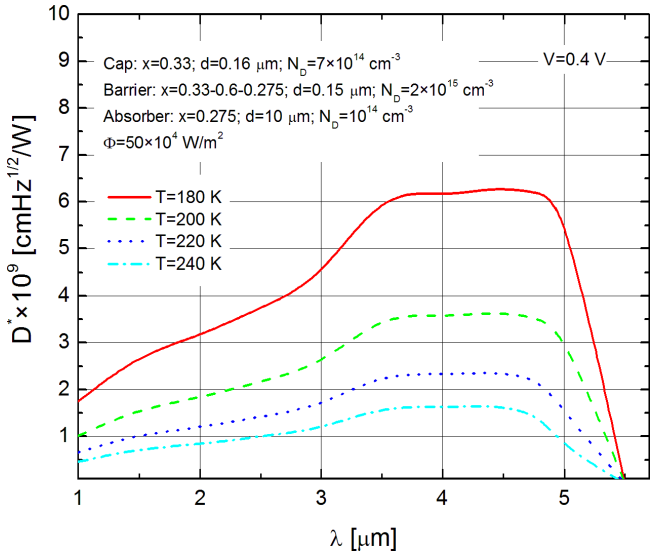

Fig. 3. D^* versus wavelength for UBIRD nBn HgCdTe/B-n type detector ($\lambda_c = 5.2$ μm at $T = 200$ K) for selected operating temperatures

3. UBIRD nBn HgCdTe/B-*n* type barrier's band alignment

The simulated energy band diagrams for unbiased and biased conditions ($V = 0.4$ V and $V = 1$ V) are depicted in Fig. 4. UBIRD HgCdTe/B-n type nBn detector is reversely biased, i.e. positive voltage is applied to the absorber contact. It is worth stressing that HgCdTe exhibits type-I heterojunction ("nested") which results in unintended valence band offset, unlike 6.1 Å $A^{III}B^{V}$ family exhibiting zero valence band offset type-II heterojunction often called "staggered". Thus, in the case of HgCdTe nBn architecture it is difficult to control band offset due to inherited "nested" band alignment [electron affinity was modelled by expression (A.2)]. Comparison of the energy band alignment between unbiased and biased structures directly indicates that UBIRD nBn HgCdTe/B-n type requires a proper level of voltage being applied to the detector (turn-on voltage) to align the valence bands (at the cap-barrier and barrier-absorber interfaces) to reduce the impediment of desirable minority carrier transport to cap layer.

Figure 5 presents cap-barrier and barrier-absorber barrier's heights (ΔE_c, ΔE_v) versus applied voltage respectively. As for as reverse biased UBIRD nBn HgCdTe detector is concerned the most crucial is ΔE_c emerging at cap-barrier interface (desirable majority carrier blocking from cap layer) and ΔE_v at barrier-absorber interface (unfavourable minority carrier hindrance). The both mentioned ΔE_c and ΔE_v barrier's heights directly depend on the applied voltage. It is clearly seen that applied voltage is a trade-off between ΔE_c and ΔE_v (e.g. for barrier-absorber interface $\Delta E_v \approx$ 120–50 meV and cap-barrier interface $\Delta E_c \approx$ 350–275 meV for $V =$ 0–1 V, respectively). Above $V = 0.4$ V (turn-on voltage level) the cap-barrier and the barrier-absorber's, ΔE_c and ΔE_v, are almost constant reaching 270 meV and 50 meV, respectively, leading to the dark and photocurrent slight increase.

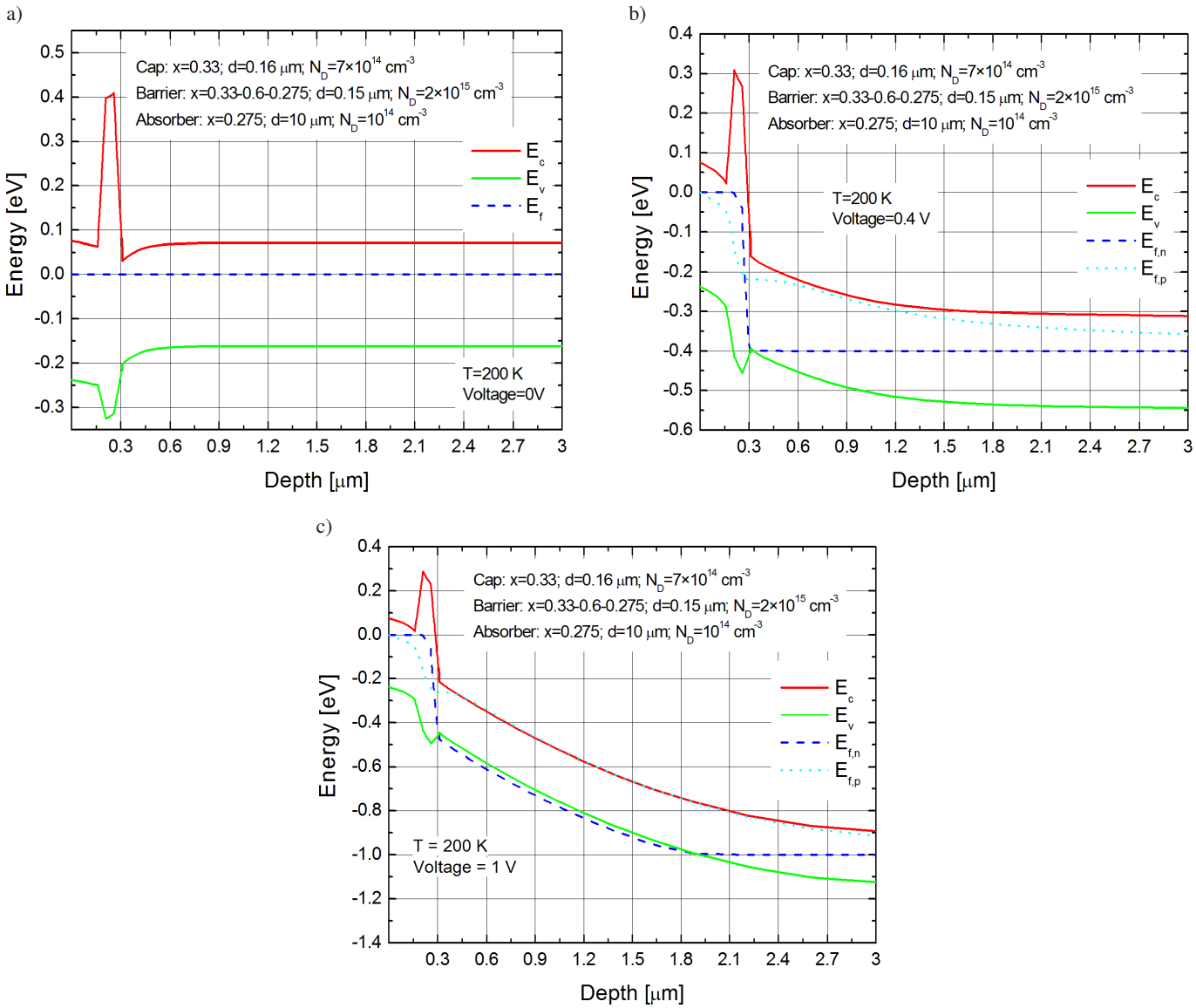

Fig. 4. Simulated energy band structures for the UBIRD nBn HgCdTe/B n-type detector at equilibrium ($V = 0$ V) (a) and under reverse biases: $V = 0.4$ V (b), $V = 1$ V (c)

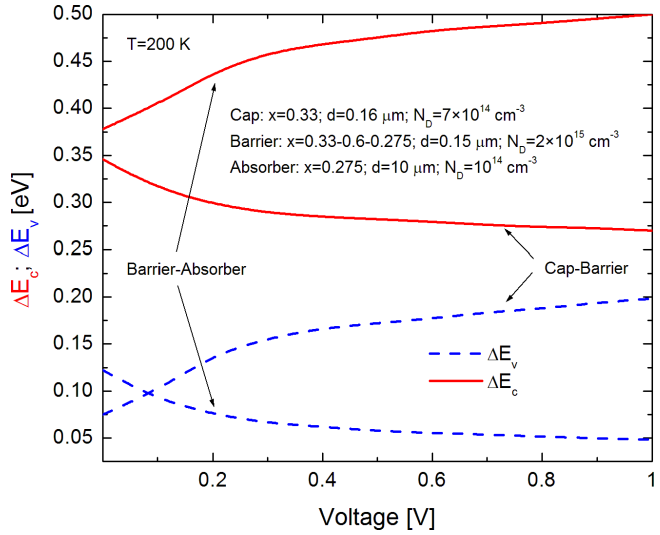

Fig. 5. ΔE_c and ΔE_v for cap-barrier and barrier-absorber interfaces versus applied voltage at $T = 200$ K

Both barrier's doping and composition also influence ΔE_c and ΔE_v. Once barrier's composition increases, ΔE_c and ΔE_v raise but ΔE_c changes more rapidly in comparison to ΔE_v, which influences detector's dark and photo currents. The increase of barrier's doping reduces cap-barrier, ΔE_c, and raises ΔE_v. The simulated ΔE_c, ΔE_v curves versus barrier's composition and doping are presented in Fig. 6.

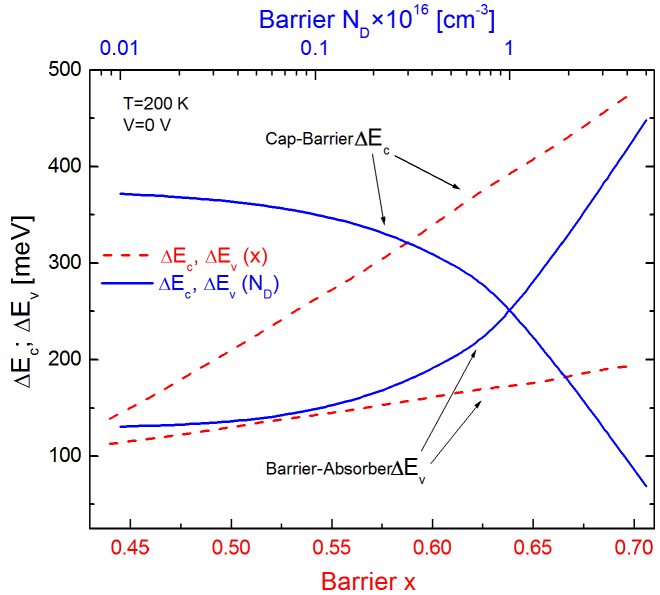

Fig. 6. ΔE_c (cap-barrier) and ΔE_v (barrier-absorber) versus barrier composition x and barriers doping for unbiased structure at $T = 200$ K

Figure 7 presents the calculated detectivity versus applied voltage at $T = 200$ K for different barrier compositions and absorber widths. Analysis of the $D^*(V, x, d)$ characteristics allowed to found optimal reverse voltage which must be applied to the structure to attain the highest detectivity (turn-on voltage). For x within the range 0.55–0.65 the optimal voltage was assumed to be $V = 0.4$ V.

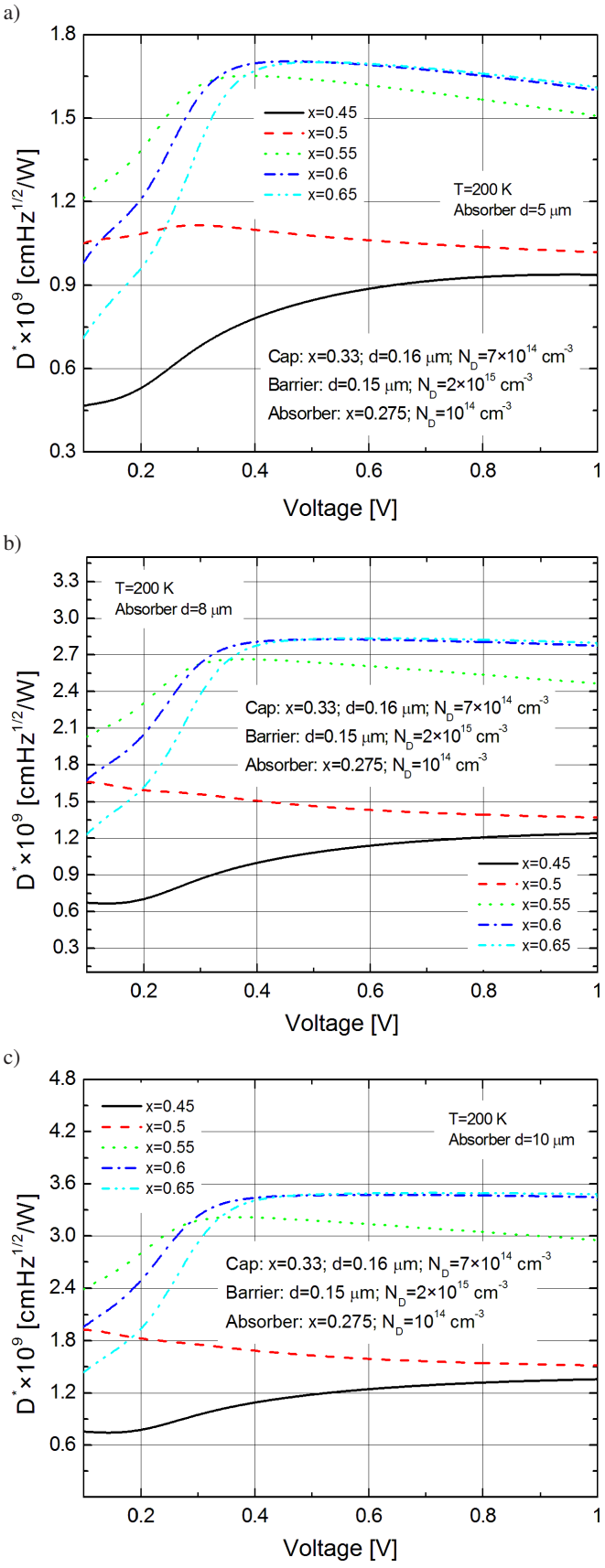

Fig. 7. Detectivity versus applied voltage for different barrier compositions, x, and absorber thickness, d

The estimated turn-on voltage is fully confirmed by the results presented in Fig. 5 and Fig. 6. The device was illuminated from cap layer side with radiation density $\Phi = 50 \times 10^4$ W/m^2 ($\lambda = 4.95$ μm). The absorption coefficient was calculated after expressions (A.9)–(A.16). The depicted results show that the highest detectivity could be reached for absorber's thickness $d = 10$ μm.

4. Optimization of the HgCdTe/B-*n* type barrier

The choice of the barrier's doping and composition plays crucial role in designing UBIRD nBn HgCdTe/B-n type structures. HgCdTe alloy's technology points out the potential issues with uniformity of the thin layers due to the interdiffusion at the interfaces. In our approach the barrier layer was divided on three sublayers with composition grading fitted to cap and absorber layers to model this adverse phenomenon (additionally gauss tail's doping profile was used, dx = 0.05 μm). For barrier's doping below $N_D < 10^{15}$ cm^{-3} and bias voltage $V > 100$ mV both dark and photocurrent slightly depend on N_D (see Fig. 8). The cap-barrier ΔE_c, and barrier-absorber, ΔE_v, keep nearly constant value for $N_D < 10^{15}$ cm^{-3} reaching 350 meV and 150 meV in average. Above $N_D > 10^{15}$ cm^{-3} photocurrent decreases which is again connected with ΔE_v raise and hole's transport is impeded to the cap layer. For voltages $V < 300$ mV characteristic minimal values of the dark current emerges while above 300 mV sharp increase of the dark current is observed. This dark current's raise is connected with the injection of the electrons from highly doped barrier to the absorber and ΔE_c decreasing versus applied voltage. In addition, the Auger 1 process contributes to the total dark current above $N_D > 5 \times 10^{15}$ cm^{-3}, while within the range $N_D = (1-5) \times 10^{15}$ cm^{-3} the number of minority carrier decreases leading to the dark current's drop. The highest detectivity could be obtained for $N_D < 3 \times 10^{15}$ cm^{-3} which is depicted in Fig. 9.

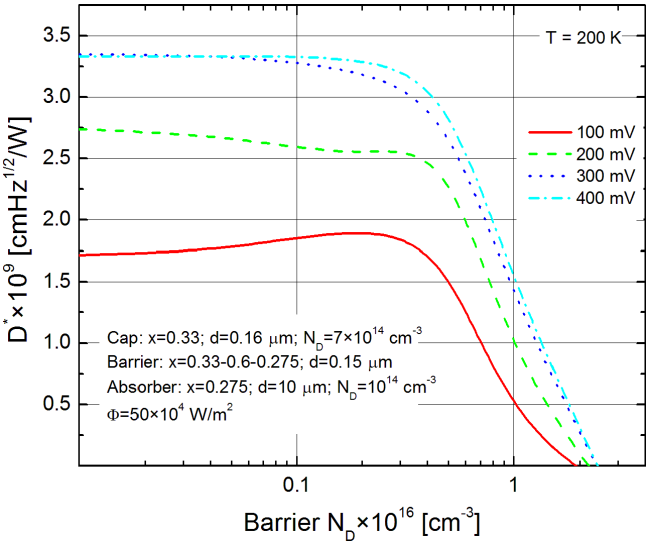

Fig. 9. D^* for UBIRD nBn HgCdTe/B-n type versus barrier doping concentration for selected voltages

Similar considerations were conducted for barrier's composition – see Figs. 10 and 11 The direct dependence of the ΔE_c and ΔE_v on composition and voltage is responsible for the both dark and photocurrent characteristics. Below $x < 0.53$ a dark current increases while a photocurrent keeps nearly a constant value. For $x > 0.53$ and $V > 200$ meV both dark and photo currents slightly decrease resulting in detectivity decreasing. Once applied voltage increases the optimal composition to attain the highest detectivity raises. The simulated structure reached $D^* = 3.3 \times 10^9$ cmHz/$^{1/2}$/W for $V = 0.4$ and $T = 200$ K, which is comparable to the result presented by Velicu *et al.* [13].

The optimal barrier thickness strictly depends on the applied bias. Once barrier's thickness increases both dark current and photocurrent decrease. For biases $V > 350$ mV upper limit of the barriers thickness was found to be $d = 0.15$ μm while for $V < 350$ mV mentioned limit reaches 0.06 μm.

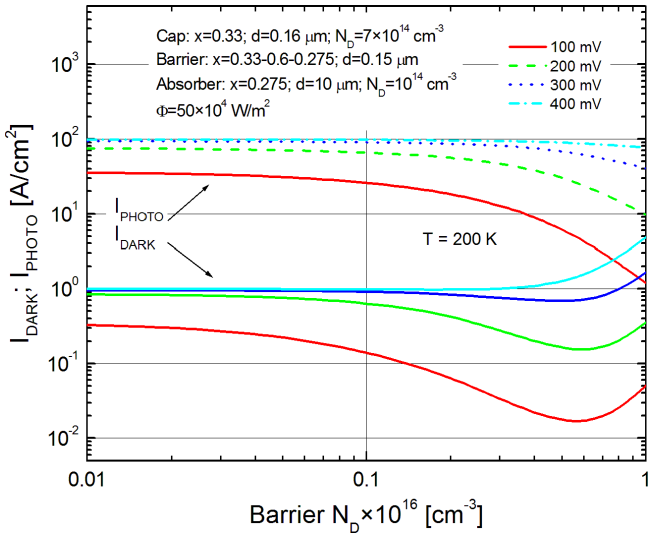

Fig. 8. I_{DARK}, I_{PHOTO} for UBIRD nBn HgCdTe/B-n type versus barrier doping concentration for selected voltages

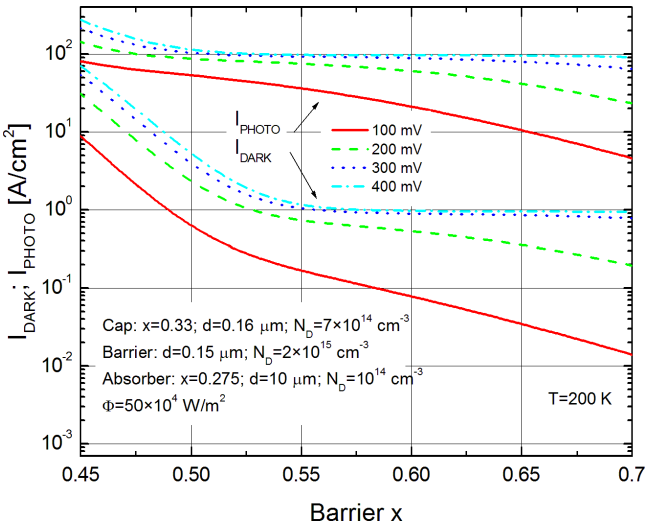

Fig. 10. I_{DARK}, I_{PHOTO} for UBIRD nBn HgCdTe/B-n type versus barrier's composition for selected voltages

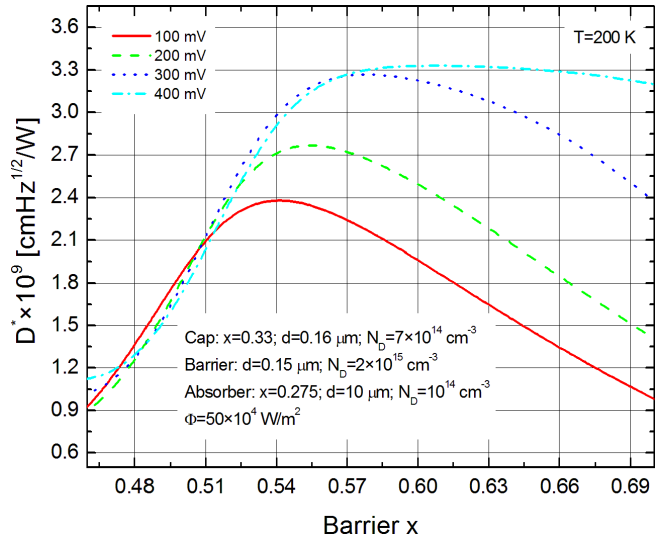

Fig. 11. D^* for UBIRD nBn HgCdTe/B-n type versus barrier's composition for selected voltages

5. Optimization of the HgCdTe/B-*n* type cap layer

Cap layer's doping and composition also influence the UBIRD nBn HgCdTe/B-n type detectors performance. It is important to correlate the barrier and absorber's composition with cap layer composition for considered voltage. For $V = 400$ mV cap layer composition may be changed within the range $0.2 < x < 0.375$ without any influence on detectivity (see Fig. 12). Once reverse voltage decreases, the cap layer composition gets more narrow assuming $0.25 < x < 0.325$ for $V = 300$ mV. Below 300 mV maximum value of detectivity could be obtained for precise cap layer composition $x = 0.225$ for $V = 200$ mV and $x = 0.2$ for $V = 100$ mV, respectively. Depending on the applied voltage and given absorber's composition ($x = 0.275$, $V = 0.4$ V) the cap's composition should meet following requirement: $x_{Cap} = x_{Absorber} + (0 \rightarrow 0.05)$. Similar considerations should be taken for cap's doping – see Fig. 13. The detectivity does not depend on the cap's doping within the range $10^{14} < N_D < 10^{16}$ cm^{-3} for analysed voltages, while above 10^{16} cm^{-3} the barrier height at cap-barrier interface decreases allowing greater number of electrons to surmount the barrier and increasing the dark current and lowering detectivity at the same time. The calculated detectivity versus selected cap's thickness shows that D^* keeps almost constant value within $d = 0.1 - 1$ μm range.

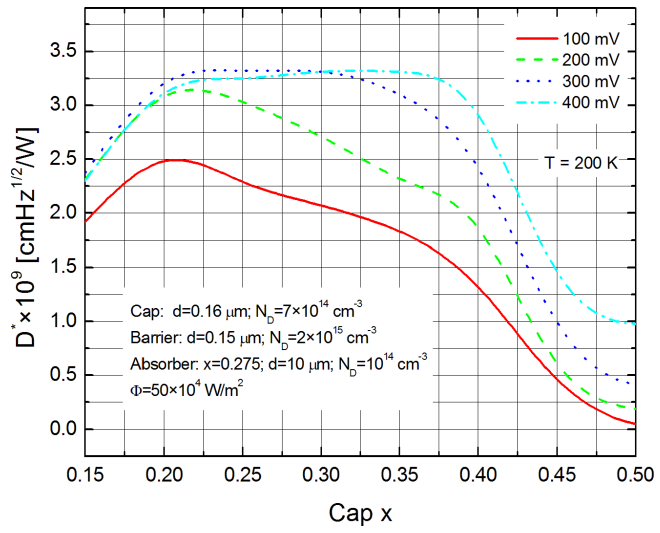

Fig. 12. D^* for UBIRD nBn HgCdTe/B-n type versus cap layer composition for selected voltages

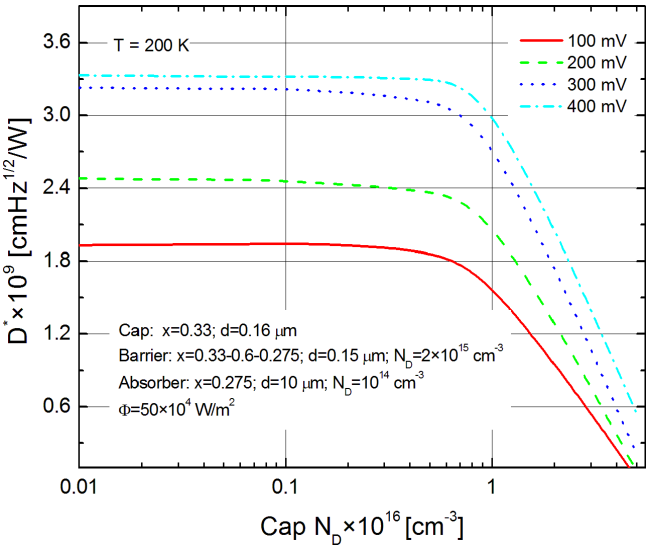

Fig. 13. D^* for UBIRD nBn HgCdTe/B-n type versus cap layer doping for selected voltages

6. Optimization of the HgCdTe/B-*n* type absorber

The absorber's doping also plays crucial role and must be optimized for assumed voltages. Once absorber's doping increases the photocurrent exhibits decreasing trend lowering responsivity ($R_i = 1.9 - 1.3$ A/W) and quantum efficiency ($\eta = 49 - 32\%$) – see Fig. 14 The barrier height ΔE_v lowers from 61 meV to 21 meV within the range of $N_D = 1 \times 10^{14}$–5×10^{16} cm^{-3} while ΔE_c changes from 290 meV to 200 mV respectively. In doping range $10^{14} < N_D < 10^{16}$ cm^{-3} the photocurrent keeps nearly constant value for simulated voltages while corresponding dark current decreases. Above $N_D = 10^{16}$ cm^{-3} the photocurrent decreases sharply which relates to the Burstein-Moss effect.

Since UBIRD nBn detector is a minority carrier device, increasing of absorber's doping causes decreasing of free hole concentration and lowering I_{DARK} (see Fig. 15). Further increase of the absorber's doping contributes to the I_{DARK} current raise due to ΔE_c lowering and Auger 1 effect. The lowest value of the $I_{DARK} = 0.2$ A/cm^2 for $V = 400$ mV could be obtained for $N_D = 5 \times 10^{15}$ cm^{-3} which corresponds to the optimal working conditions.

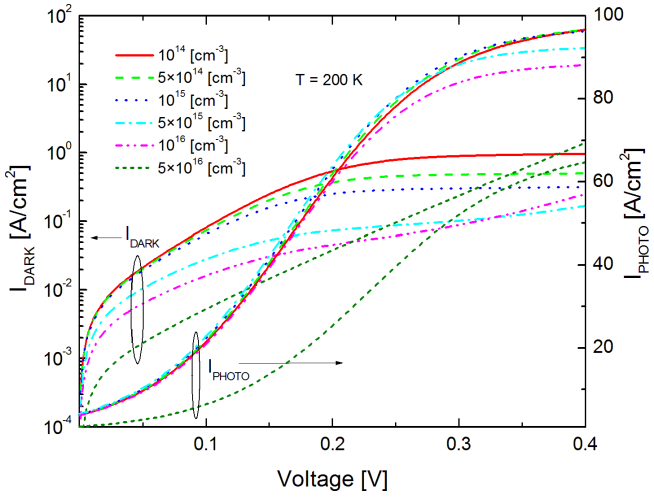

Fig. 14. I_{DARK} and I_{PHOTO} for UBIRD nBn HgCdTe/B-n type detector versus bias voltage for different absorber's doping. $T = 200$ K

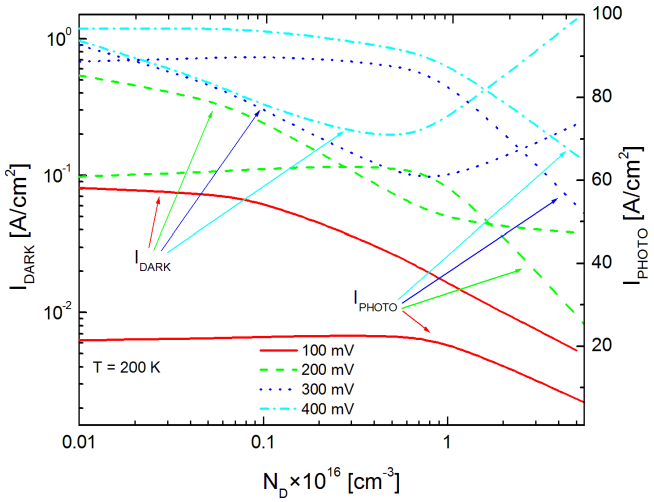

Fig. 15. I_{DARK} and I_{PHOTO} for UBIRD nBn HgCdTe/B-n type detector versus absorber's doping for different bias voltages. $T = 200$ K

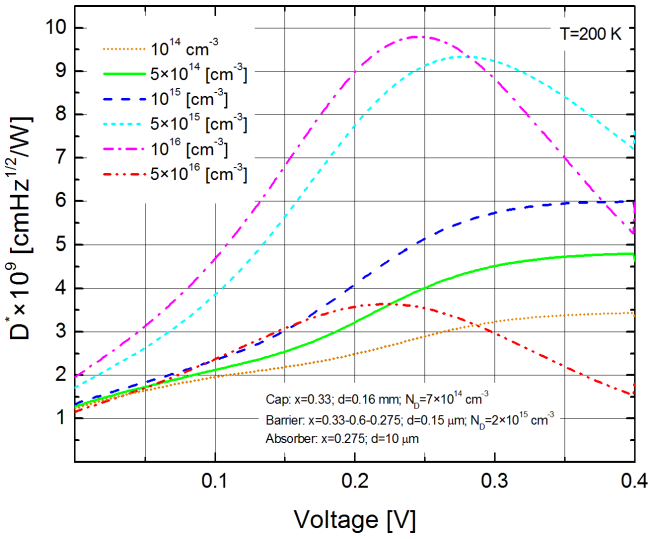

Fig. 16. Detectivity for UBIRD nBn HgCdTe/B-n type versus applied voltage for selected absorber's doping concentrations

Figure 16 presents D^* versus voltage for selected absorber's doping. The presented results indicate that the maximum value of the $D^* = 10^{10}$ cmHz$^{1/2}$/W for given structure could be obtained for absorber's doping $N_D = 10^{16}$ cm^{-3} and $V = 250$ mV while above 10^{16} cm^{-3} the detectivity decreases rapidly due to dark current increasing and lowering of the photocurrent. For $V = 0.4$ V the highest detectivity is attained for $N_D = 5 \times 10^{15}$ cm^{-3} and reaches $D^* = 7 \times 10^9$ cmHz$^{1/2}$/W. Once absorber's doping increases, the optimal bias voltage applied to the structure decreases. As it is shown in Fig. 7, the absorber thickness influences the IR absorption leading to the higher detectivities for the larger absorber's thickness.

7. Comparison of the detectors' technologies

The very last figure (Fig. 17) compares the R_oA and RA products versus temperature for the MWIR nBn HgCdTe/B-n type, InAs/GaSb/B-AlGaSb T2SL nBn ($\lambda_c = 5.4$ μm) detector, InAs/GaSb PIN photodiode ($\lambda_c = 6.2$ μm), and HOT HgCdTe bulk photodiodes ($\lambda_c = 5.4$ μm) fabricated at the common Military University of Technology and Vigo System Laboratory. The theoretical simulation of the T2SLs InAs/GaSb/B-AlGaSb nBn detector is presented in Ref. 14 and Ref. 15, where an analytical approach was used to model the detectors's performance, while T2SLs PIN photodiodes state of art was analysed by Wróbel *et al.* [16]. It is clearly seen that the performance of UBIRD nBn HgCdTe/B-n type has reached a comparable level with the state of the art T2SLs nBn, PIN detectors and HOT HgCdTe bulk photodiodes. In fact, the RA products of MWIR 5.2-μm HgCdTe/B-n type and 5.4-μm T2SLs nBn devices are comparable with bulk HgCdTe photodiodes, but they were measured at $V = 50$ mV reverse bias, whereas the RA product of 6.2-μm T2SL PIN photodiode is measured at reverse bias conditions ($V = 200$ V). The HgCdTe bulk photodiodes exhibit a better performance mainly due to the higher quantum efficiency ($\eta = 50$–70%).

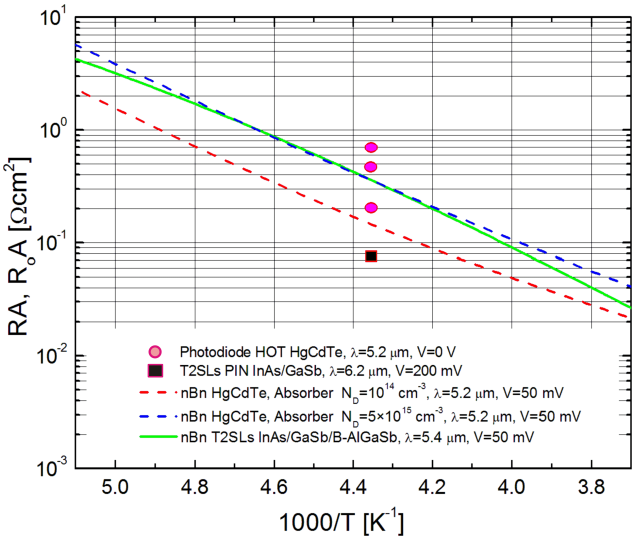

Fig. 17. Temperature dependence of the RA and R_oA products for MWIR HgCdTe/B-n type nBn detector, InAs/GaSb/B-$Al_{0.2}Ga_{0.8}Sb$ T2SL nBn detector, HgCdTe HOT bulk diodes and InAs/GaSb T2SL PIN diodes operating at near-room temperature

8. Conclusions

In the paper we simulated the performance of the MWIR nBn HgCdTe/B-n type detector versus operating conditions and structural parameters. The unfavourable compositional uniformity and interdiffusion at the interfaces were modelled by the proper barrier grading matched to the cap and absorber's composition respectively. The maximum *RA* product of the detector with 5.2 μm cut-off wavelength is higher than 0.1 Ωcm^2 at 230 K, while maximum detectivity was estimated to be (3–10)$\times 10^9$ cmHz$^{1/2}$/W at $T = 200$ K depending on absorber's doping and applied bias. Inherited barriers in both conduction and valence bands were analysed in detail pointing the optimal operating conditions as for as bias and doping are concerned. The turn-on voltage above which a dark current increases slowly was estimated to be $V = 0.4$ V.

Even though, it is difficult to attain desirable band alignment in the valence band, the proposed UBIRD nBn HgCdTe/B-n structure and its performance paves the way for the development of unipolar devices. In addition, analysed structure allows circumventing requirements for p-type doping reducing number of the processing steps. Barrier's doping and composition should be perceived as the most important parameters in UBIRD HgCdTe/B-n type nBn structure optimization. The proper doping and composition choice leads to either building up or lowering the barriers in both conduction and valence bands.

As stated above, it is well-known, that T2SL InAs/GaSb 6.1 Å compound family is the only one infrared material system theoretically predicted to achieve higher performance than the HgCdTe bulk photodiodes. However, so far the HOT HgCdTe photodiode performance has not been overcome by T2SL PIN and nBn detectors because of the low quantum efficiency and presence of the SRH recombination characterized by a relatively short carrier lifetime. The mentioned limitations could be circumvented by simplified structures UBIRD HgCdTe/B-n nBn type. Finally, unlike T2SLs InAs/GaSb/BAlGaSb nBn detector, UBIRD HgCdTe/B-n nBn type does not require highly doped layers which should be perceived as a technological advantage.

Appendix

The UBIRD nBn HgCdTe/B-n type detector was simulated using the following material parameters [1, 17]:

Band-gap energy:

$$E_g(x,T) = -0.302 + 1.93x - 0.81x^2 + 0.832x^3 + 5.35\times 10^{-4}T(1-2x). \tag{A.1}$$

Electron affinity:

$$\gamma = 4.23 - 0.813(E_g(x,T) - 0.083). \tag{A.2}$$

Carriers' effective masses:

$$m_e^* = 8.035\times 10^{-2}E_g(x,T)m_o, \tag{A.3}$$

$$m^* + h = 0.55m_o. \tag{A.4}$$

Dielectric constant:

$$\varepsilon = 20.5 - 15.5x + 5.7x^2. \tag{A.5}$$

The radiative recombination rate:

$$B = 5.9052\times 10^{18}n_i^{-2}\varepsilon T^{3/2}\sqrt{\frac{1+x}{(81.9+T)}}\exp\left(-\frac{E_g}{k_BT}\right)(E_g^2 + 3k_BTE_g + 3.75k_B^2T^2). \tag{A.6}$$

The Auger recombination coefficients C_n and C_p:

$$C_n = 5\times 10^{-12}\,|F_1F_2| \cdot \left[\left(\frac{E_g}{k_BT}\right)^3\exp\left(1+2\frac{m_e^*}{m_h^*}\right)\left(\frac{E_g}{k_BT(m_e^*/m_h^*)}\right)\right]^{-1/2} \times n_i^{-2}\left[3.8\times 10^{-18}\varepsilon^2\left(\frac{1}{m_e^*}\right)\left(1+2\frac{m_e^*}{m_h^*}\right)\sqrt{1+\frac{m_e^*}{m_h^*}}\right]^{-1}, \tag{A.7}$$

$$C_p = 0.1C_n. \tag{A.8}$$

The absorption coefficient:
for: $\lambda > \lambda_c$

$$\alpha = \alpha_o\left[\frac{\alpha_g}{\alpha_o}\right]^{\xi}, \tag{A.9}$$

$$\xi = \frac{1.24/\lambda_c - e_o}{e_g - e_o}, \tag{A.10}$$

for: $\lambda \le \lambda_c$

$$\alpha = \alpha_g\exp\left(\sqrt{B(1.24/\lambda_c - e_g)}\right), \tag{A.11}$$

$$e_g = -0.295 + 1.87x - 0.28x^2 + (6 - 14x + 3x^2)\times 10^{-4}T + 0.35x^4, \tag{A.12}$$

$$\alpha_g = -65 + 1.883T + (8694 - 10.314T)x, \tag{A.13}$$

$$\alpha_o = \exp(-18.5 + 45.68x), \tag{A.14}$$

$$e_o = -0.355 + 1.77x, \tag{A.15}$$

$$B = \sqrt{(-1 + 0.083T + (21 - 0.13T)x)}. \tag{A.16}$$

Acknowledgements. This paper has been done under financial support of the Polish National Science Centre, Project: DEC-2011/01/B/ST5/06283.

REFERENCES

[1] A. Rogalski, *Infrared Detectors*, second edition, CRC Press, Boca Raton, 2011.
[2] A. Rogalski, "HgCdTe infrared detector material: history, status and outlook", *Rep. Prog. Phys.* 68, 2267–2336 (2005).
[3] P. Norton, "HgCdTe infrared detectors", *Opto-Electron. Rev.* 10, 159–174 (2002).
[4] A. Rogalski and P. Martyniuk, "InAs/GaInSb superlattices as a promising material system for third generation infrared detectors", *Infrared Physics & Technol.* 48, 39–52 (2006).
[5] D.Z. Ting, C.J. Hill, A. Soibel, J. Nguyen, S. Keo, M.C. Lee, J.M. Mumolo, J.K. Liu, and S.D. Gunapala, "Antimonide-based barrier infrared detectors", *Proc. SPIE* 7660, 76601R (2010).

[6] D.Z.-Y. Ting, A. Soibel, L. Höglund, J. Nguyen, C.J. Hill, A. Khoshakhlagh, and S.D. Gunapala, "Type-II superlattice infrared detectors", in *Semiconductors and Semimetals*, eds. S.D. Gunapala, D.R. Rhiger, and C. Jagadish, Vol. 84, pp. 1–57, Elsevier, Amsterdam, 2011.

[7] P. Klipstein, "XBn barrier photodetectors for high sensitivity and high operating temperature infrared sensors", *Proc. SPIE* 6940, 69402U-1–11 (2008).

[8] S. Maimon and G. Wicks, "nBn detector, an infrared detector with reduced dark current and higher operating temperature", *Appl. Phys. Lett.* 89, 151109-1–3 (2006).

[9] J.B. Rodriguez, E. Plis, G. Bishop, Y. D. Sharma, H. Kim, L.R. Dawson, and S. Krishna, "nBn structure based on InAs/GaSb type-II strained layer superlattices", *Appl. Phys. Lett.* 91, 043514-1–2 (2007).

[10] P. Martyniuk, A. Rogalski, "Comparison of performance of quantum dot and other types infrared photodetectors", *Proc. SPIE* 6940, 694004 (2008).

[11] P. Martyniuk, A. Rogalski, "Insight into performance of quantum dot infrared photodetectors", *Bull. Pol. Ac. Tech.* 57, 103-116 (2009).

[12] A. M. Itsuno, J. D. Philips, and S. Velicu, "Design and modeling of HgCdTe nBn detectors", *J. Elect. Mater.* 40, 9 (2011).

[13] S. Velicu, J. Zhao, M. Morley, A.M. Itsuno, and J.D. Philips, "Theoretical investigation of MWIR HgCdTe nBn detectors", *Proc. SPIE.* 8268, 82682X (2012).

[14] P. Martyniuk, J. Wrobel, E. Plis, P. Madejczyk, A. Kowalewski, W. Gawron, S. Krishna, and A. Rogalski, "Performance modeling of MWIR InAs/GaSb/B–$Al_{0.2}Ga_{0.8}Sb$ type-II superlattice nBn detector", *Semicond. Sci. Technol.* 27, 055002 (2012).

[15] J. Wróbel, P. Martyniuk, E. Plis, P. Madejczyk, W. Gawron, S. Krishna, and A. Rogalski, "Dark current modeling of MWIR type-II superlattice detectors", *Proc. SPIE* 8353, 8353-16 (2012).

[16] J. Wrobel, P. Martyniuk, E. Plis, P. Madejczyk, W. Gawron, S. Krishna, and A. Rogalski, "Analysis of temperature dependence of dark current mechanisms for middle wavelength infrared InAs/GaSb superlattice photodiodes", (2013), to be published.

[17] *APSYS Macro/User's Manual ver. 2011*, Crosslight Software, Inc., 2011.